

# Role of Microstructure in Dielectric Properties of Thermally Sprayed Ceramic Coatings

Minna Niittymäki, Ilkka Rytöluoto and Kari Lahti

Department of Electrical Engineering

Tampere University of Technology

Tampere, Finland

minna.niittymaki@tut.fi

Jarkko Metsäjoki and Tomi Suhonen

Thermal Spray, Advanced Materials

VTT Technical Research Centre of Finland

Espoo, Finland

**Abstract**— Thermally sprayed insulating ceramic coatings can be utilized in conditions where polymers are inapplicable. The coatings exhibit a special lamellar microstructure with interfaces and some defects (e.g. voids, cracks) in between. The aim of this study was to analyze the relationship between the microstructural features and the dielectric properties of various thermally sprayed ceramics. The structural characterization of the ceramic coatings was made based on following properties: porosity, volumetric gas permeability and the characteristic size of crystalline lamella. High gas permeability of the coatings decreased the breakdown strength but similar effect cannot be seen in the DC resistivity and the permittivity results. Decrease of DC resistivity at high humidity did not correlate to microstructural properties; rather it is speculated to indicate the hydrophilic nature of the coatings. The characteristic crystalline domain sizes showed no clear correlation with the dielectric properties.

**Keywords**—*thermal; spray; ceramic; coating; alumina; spinel; resistivity; permittivity; breakdown; microstructure; porosity*

## I. INTRODUCTION

Thermally sprayed insulating ceramic coatings can be utilized in conditions where polymers are inapplicable. In order to use the coatings in real applications, the role of microstructural features in the dielectric properties has to be known. The coatings are deposited in layers forming a lamellar structure consisting of interfaces and some defects (e.g. voids and cracks) [1]–[3]. Especially, the cracks enable easier charge carrier movement [4] which is problematic for insulating coatings.

Typically, porosity is used to characterize the microstructure of thermally sprayed ceramic coatings. The determination of the porosity can be made by using several methods [5]. Typical method is image analysis which is made by using cross-sectional micrographs taken by optical or scanning electron microscopes [3]–[7]. Although the image analysis gives a good estimation about the porosity [5], the defined value does not represent the volumetric porosity of a coating which would take into consideration the unique shape of the voids which have influence on the mechanical properties of the coatings [3]. However, the shape and orientation of the pores can be defined by using 3-dimensional images instead of the 2D images [8], [9] but the analyzing methods are not as widely used as the methods based on the 2D images. Anyhow,

the porosity cannot be the only structural parameter to determine the microstructure of the coatings, and quantitative methods are also required [3].

The influence of the microstructural features on the dielectric properties have been discussed previously in [1], [6] in which the high porosity has been suggested to decrease the breakdown strength. However, it has been also reported that porosity does not clearly affect the breakdown strength of thermally sprayed coatings [7], [10], [11]. In addition, the size of the lamella and the amount of amorphous areas has been discussed to affect the dielectric losses at low frequencies and DC conductivity but the analysis was made only visually [11]. The aim of this paper is to link several microstructural features (porosity, gas permeability, the size of lamella) to the dielectric properties of various thermally sprayed ceramic coatings.

## II. EXPERIMENTAL

### A. Material characterization

Six different experimental MgO–Al<sub>2</sub>O<sub>3</sub> powders were sprayed by high-velocity oxygen fuel (HVOF)–thermal spray method on stainless steel substrates. The amount of MgO in the powder varied from 0 mol% to 65 mol%. Detailed information of the studied coatings is given in Table 1. The coating thickness was determined either by using magnetic measuring device (Elcometer 456B) or from cross-sectional images taken by optical microscopy (Table 1). The high standard deviation in thickness is partly due to the grit-blasting made for the steel substrates in order to ensure good adhesion between the ceramic and the steel.

The porosities of the coatings were determined by analyzing cross-sectional micrographs taken by optical microscopy (OM, 320× magnification) and by scanning electron microscope (SEM, 1000× magnification) using both secondary electron detector (SE) and backscattered electron detector (BSE), see Table 1. The porosities were determined as the ratio of total area of voids to the total image area. In addition to image analysis, the gas (nitrogen) permeability (GP) was measured for the coatings, providing an indirect measure of the porosity with a higher gas permeability indicating a higher porosity.

In order to analyze the lamellar morphologies, the SEM/BSE images were converted into binary pixel matrices

TABLE I. POWDER COMPOSITIONS OF THE STUDIED HVOF COATINGS, THE DEFINED POROSITIES, THICKNESSES AND CRYSTALLINE LAMELLA THICKNESS ( $L_f$ ).

Sample	Powder composition	$L_f$ (μm)	Porosity				Thickness (μm)		
			OM (%)	SEM/SE (%)	SEM/BSE (%)	GP (nm <sup>2</sup> )	From cross-section image	From magnetic measurement	SD
HVOF7	100 mol% Al <sub>2</sub> O <sub>3</sub>	2.184	2.9	1.0	2.6	7.71	255	237	10.2
HVOF8	90 mol% Al <sub>2</sub> O <sub>3</sub> – 10 mol% MgO	2.157	3.0	1.2	3.1	4.76	195	193	8.0
HVOF9	75 mol% Al <sub>2</sub> O <sub>3</sub> – 25 mol% MgO	1.507	2.5	1.2	3.1	3.86	190	184	7.9
HVOF10	60 mol% Al <sub>2</sub> O <sub>3</sub> – 40 mol% MgO	2.463	3.1	1.1	3.0	13.3	235	241	13.8
HVOF11	50 mol% Al <sub>2</sub> O <sub>3</sub> – 50 mol% MgO	1.697	2.4	1.1	3.8	6.27	257	215	2.4
HVOF12	35 mol% Al <sub>2</sub> O <sub>3</sub> – 65 mol% MgO	1.460	2.3	1.6	3.8	15.5	191	234	10.0

corresponding to the crystalline and amorphous areas and analyzed quantitatively in MATLAB. In accordance with the free-space length developed by Khare & Burris [12], quantitative determination of the characteristic size of a morphological domain of interest provides means to relate structural features and material properties. In this paper, the free-space length,  $L_f$ , was utilized to characterize the size of the crystalline domains of the coatings. Free-space length can be defined as the size of the largest randomly placed box for which the most probable number of intersecting pixels corresponding to amorphous regions is zero. The MATLAB code, retrieved and used according to the literature [12], [13], iterates to box size by Monte Carlo approach—a more thorough description of the method is presented in [12], [13].

### B. Dielectric characterization

For DC resistivity and permittivity measurements, a round electrode ( $\varnothing=50$  mm) was painted on the sample surface using a silver paint (SPI High Purity Silver Paint). In addition, a shield electrode was painted around the measuring electrode to neglect possible surface currents. For breakdown measurements, smaller silver painted electrodes ( $\varnothing=11$  mm) were prepared. After painting the electrodes, the samples were at first dried at 120 °C for two hours followed by conditioning at a climate room at 20 °C/RH 20 % for at least 12 h before the measurements. All the measurements were also performed at the formerly mentioned conditions in the climate room.

DC breakdown voltage measurements were performed with linearly increased DC voltage (100 V/s) using methods depicted in [14]. Oil immersion was not used in the measurements because the coatings are porous allowing oil to penetrate into the coating which significantly affects the breakdown strength [14]. During the breakdown (BD) tests, a stainless steel rod electrode ( $\varnothing=11$  mm) was placed on the top of the painted electrode while the stainless steel substrate acted as the other electrode. Dielectric breakdown strength (DBS) was calculated by dividing the breakdown voltage by the coating thickness at the painted electrode location.

Typically dielectric breakdown strength of solid materials is Weibull distributed and due to this the results were fitted to this distribution. The cumulative density function of a two-parameter Weibull distribution is given as

$$F(x, \alpha, \beta) = 1 - \exp \left\{ \left( \frac{x}{\alpha} \right)^{\beta} \right\} \quad (1)$$

where  $F(x)$  is the breakdown probability,  $x$  is the measured breakdown strength (V/μm),  $\alpha$  is the scale parameter (V/μm) and  $\beta$  is the shape parameter. The scale parameter represents the breakdown strength at the 63.2 % failure probability and

the shape parameter indicates the slope of the theoretical distribution. The statistical analysis was performed using Weibull++ software and the Maximum Likelihood method was used in the parameter estimation.

Resistivity measurements were made using Keithley 6517B electrometer. In order to study the resistivity as a function of applied electric field, the test electric field varied from ~0.1 V/μm to ~5 V/μm. The test voltage was maintained for a time period of 1000 s at each voltage step. The resistivity was defined from the stabilized current value in the end of the measurement period. All the measuring arrangements were in accordance with the IEC standard 60093.

Relative permittivity and dielectric losses of the material were studied with an insulation diagnostic analyzer device (IDA 200,  $U_{\max}=200$  V<sub>peak</sub>). During the measurements, a sinusoidal voltage (200 V<sub>peak</sub>) with varying frequency (1 kHz–0.1 Hz) was applied over the sample. The permittivity of a coating was calculated using the equivalent parallel RC-circuit. All the test arrangements were performed in accordance with the IEC standard 60250.

## III. RESULTS AND DISCUSSION

### A. Structural analysis

Exemplifying SEM/BSE cross-sectional morphologies are presented in Fig. 1, showing the porous nature and the lamellar crystal structure of the coatings. While the porosities determined from the cross-sectional micrographs were found to be relatively similar for all the coatings, the gas permeability measurements indicated significant differences between the coatings, see Table I. This is most likely due to the fact that gas permeability provides a more accurate estimate of the volumetric porosity than a single cross-sectional micrograph. It is noted that the varying amount of small vertical cracks visible in the cross-sectional images likely contribute to porosity and gas permeability, with this being most prominent for HVOF10 which exhibited particularly long vertical cracks (see Fig. 1 and Table I). Fig. 1 also presents the corresponding binary images utilized for quantitative determination of the characteristic crystalline domain size and the calculated free-space lengths. While HVOF9 and HVOF12 were found to exhibit slightly more compact amorphous–crystalline regions, the overall differences remained small and showed no clear correlation with the MgO-content.

### B. DC breakdown strength

Breakdown voltage measurements were performed for 15 parallel samples of each coating. The breakdown strength of the coatings is presented in Fig. 2. The highest breakdown strengths were obtained for HVOF9 (25 % MgO) and HVOF8 (10 % MgO) while the lowest breakdown strengths were

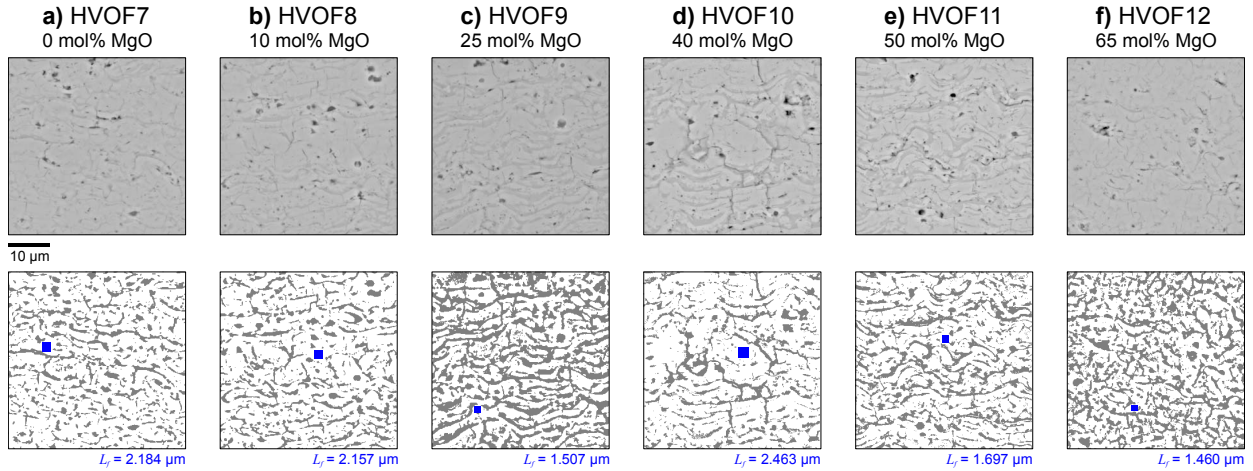


Fig. 1. Zoomed-in portions of the SEM/BSE cross-sectional images of the studied coatings at 1000 $\times$  magnification. The total studied image areas were 121 $\times$ 98  $\mu\text{m}^2$ . The top row presents the original SEM images, with light gray, dark gray and black image regions corresponding to the crystalline, amorphous and void (porosity) regions. The bottom row presents the corresponding binary images utilized for the quantitative structural analysis. The free-space length,  $L_f$ , characterizing the size of the crystalline domain is presented in each figure. Free-space length determination was performed iteratively in MATLAB (in manual mode) by gradually increasing the amount of random tests up to 100,000 in order to obtain high statistical accuracy.

measured for HVOF12 (65 % MgO) and HVOF10 (40 % MgO). Interestingly, the breakdown strength of the alumina (HVOF7, 0 % MgO) and spinel (HVOF11, 50 % MgO) is very similar although typically the HVOF spinel coatings exhibit higher breakdown strength than the HVOF alumina coatings [6], [11].

The significant difference between the lowest and the highest DBS can be explained by the differences in gas permeabilities. The relationship between the GP and breakdown strength is presented in Fig. 2 in which the Weibull parameters ( $\alpha$  &  $\beta$ ) are shown as a function of gas permeability. It was noted that a coating with a high GP value also showed lower breakdown strength. On the other hand, the characteristic crystalline domain sizes showed no clear correlation with the breakdown strength, which suggests that the porosity and the vertical cracks (structural defects) play a more determining role in the DBS of the coating than the crystalline–amorphous morphology, in coherence with [1], [6]. It is also remarked that the observed long vertical cracks, particularly in HVOF10, likely affect the DBS. However, a more detailed analysis of the amount and size of the cracks is not presented in this paper.

Obviously, the amount of MgO has also some effect on the breakdown strength. However, this effect is difficult to obtain comparing the breakdown strengths because HVOF10 (40 %

MgO) exhibit long vertical cracks and high GP in comparison to the HVOF9 (25 % MgO) and HVOF11 (50 % MgO). Even though, it can be noticed that 10 % or 25 % MgO content in a coating produced the highest breakdown strength. When the MgO amount is 0 % or 50%, the breakdown strength is lower. However, the breakdown strengths of HVOF7 and HVOF11 (39.2 V/ $\mu\text{m}$  and 40.3 V/ $\mu\text{m}$ , respectively) is well in line with our previous studies [11], [14].

### C. DC resistivity

DC resistivity as a function of electric field is presented in Fig. 3a). The lowest resistivity was measured for HVOF7 (100 %  $\text{Al}_2\text{O}_3$ ). When 10 % MgO was mixed with  $\text{Al}_2\text{O}_3$ , the resistivity increased slightly (HVOF8). The DC resistivities of the coatings (HVOF9–HVOF12) were practically at similar level. In addition, the non-ohmic behavior cannot be seen for these coatings at the studied field strengths, however the HVOF7 and HVOF8 exhibit the typical non-ohmic behavior of thermally sprayed ceramic coatings [11], [15].

In order to study the effect of high humidity on the DC resistivity of the coatings, DC resistivity (2–4 V/ $\mu\text{m}$ ) was measured for the coatings HVOF8–HVOF12 at 20 °C/RH 90 % conditions. The resistivity decreased  $\sim$ 5 decades. The difference could not be seen to correlate with any of the

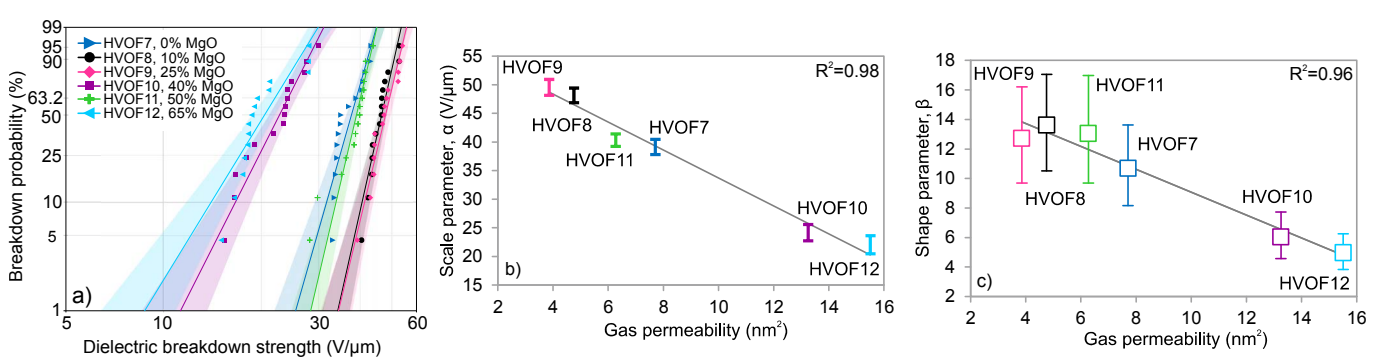


Fig. 2. a) DC breakdown strength of the coatings in Weibull probability plot where the shaded areas present 90 % confidence bounds. b)–c) Weibull parameters  $\alpha$  and  $\beta$  as a function of gas permeability where the error bars present the 90 % confidence bounds for the parameters.

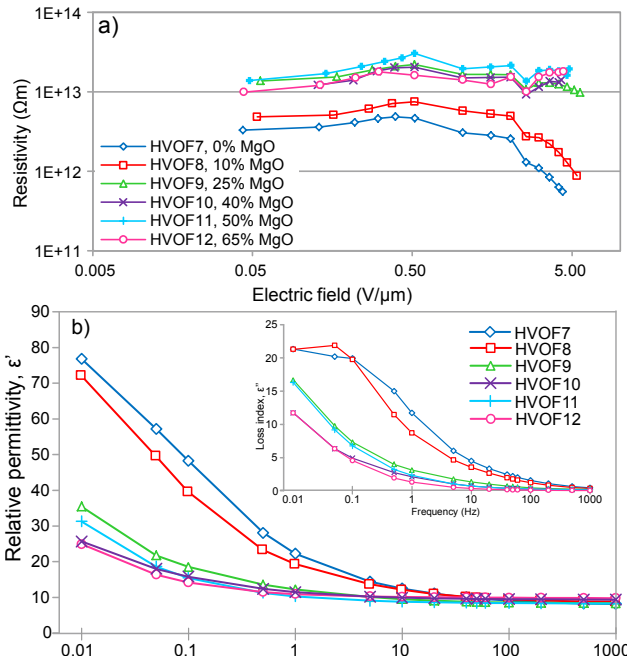


Fig. 3. a) DC resistivity as a function of electric field b) relative permittivity for the studied coatings and the loss index  $\epsilon''$  as a function frequency (inset).

defined microstructural parameters, like gas permeabilities. Similar decrease in resistivity was also reported in [6] in which the DC resistivity was measured for HVOF alumina and spinel coatings which were kept in RT/RH ~95 % conditions for 48 h before the resistivity measurements. In [6], it was discussed that the coatings are sensitivity to humidity due to the nature of the material, the microstructure and the phase composition. Thus, it can be speculated that the hydrophilic nature of the coatings has more significant effect on the DC resistivity than long vertical cracks or high gas permeability.

#### D. Relative permittivity and dielectric losses

The relative permittivity ( $\epsilon'$ ) and the loss index ( $\epsilon''$ ) of the studied coatings as a function of frequency is shown in Fig. 3b). At frequencies from 20 Hz to 1 kHz, the relative permittivity is at similar level for all the coatings. Below 10 Hz differences exist, the HVOF7 and HVOF8 having the highest permittivities. The permittivities of the coatings HVOF9–HVOF12 are more or less at same level. The loss indices of HVOF7 and HVOF8 are significantly higher than those of the other coatings. The losses of HVOF9–HVOF12 are also at a similar level. Thus, the loss index results are well in line with the DC resistivity results. However, no coherence with any of the defined microstructural features (e.g. gas permeability) can be seen in permittivity or in loss index.

#### IV. CONCLUSIONS

The structural characterization of thermally sprayed ceramic coatings was made based on following properties: porosity, volumetric gas permeability and the size of characteristic crystalline lamella. High gas permeability of the coatings decreased the breakdown strength but similar effect cannot be seen in the DC resistivity and the permittivity results.

It was also remarked that the observed long vertical cracks likely affected the breakdown strength. Decrease of DC resistivity at high humidity did not correlate to microstructural properties; rather it is speculated to indicate the hydrophilic nature of the coatings. The characteristic crystalline domain sizes showed no clear correlation with the dielectric properties.

#### REFERENCES

- [1] L. Pawłowski, "The relationship between structure and dielectric properties in plasma-sprayed alumina coatings," *Surf. Coatings Technol.*, vol. 35, no. 3–4, pp. 285–298, 1988.
- [2] L. Pawłowski, *The Science and Engineering of Thermal Spray Coatings*. Chichester, West Sussex, England: John Wiley & Sons Ltd, 2008.
- [3] C.-J. Li and A. Ohmori, "Relationships between the microstructure and properties of thermally sprayed deposits," *J. Therm. Spray Technol.*, vol. 11, no. 3, pp. 365–374, 2002.
- [4] S. Beauvais, V. Guipont, F. Borit, M. Jeandin, M. Espaňol, K. A. Khor, A. Robisson, and R. Saenger, "Process-microstructure-property relationships in controlled atmosphere plasma spraying of ceramics," *Surf. Coatings Technol.*, vol. 183, no. 2–3, pp. 204–211, May 2004.
- [5] S. Deshpande, A. Kulkarni, S. Sampath, and H. Herman, "Application of image analysis for characterization of porosity in thermal spray coatings and correlation with small angle neutron scattering," *Surf. Coatings Technol.*, vol. 187, no. 1, pp. 6–16, Oct. 2004.
- [6] F. L. Toma, S. Scheitz, L. M. Berger, V. Sauchuk, M. Kusnezoff, and S. Thiele, "Comparative study of the electrical properties and characteristics of thermally sprayed alumina and spinel coatings," *J. Therm. Spray Technol.*, vol. 20, no. 1–2, pp. 195–204, 2011.
- [7] J. Kotlan, R. C. Seshadri, S. Sampath, P. Ctibor, Z. Pala, and R. Musalek, "On the dielectric strengths of atmospheric plasma sprayed Al2O3, Y2O3, ZrO2–7% Y2O3 and (Ba,Sr)TiO3 coatings," *Ceram. Int.*, vol. 41, no. 9, pp. 11169–11176, Nov. 2015.
- [8] S. Beauvais, V. Guipont, M. Jeandin, D. Jeulin, A. Robisson, and R. Saenger, "Study of the Porosity in Plasma-Sprayed Alumina through an Innovative Three-Dimensional Simulation of the Coating Buildup," *Metall. Mater. Trans. A*, vol. 39, no. 11, pp. 2711–2724, Jul. 2008.
- [9] O. Amsellem, F. Borit, D. Jeulin, V. Guipont, M. Jeandin, E. Boller, and F. Pauchet, "Three-dimensional simulation of porosity in plasma-sprayed alumina using microtomography and electrochemical impedance spectrometry for finite element modeling of properties," *J. Therm. Spray Technol.*, vol. 21, no. 2, pp. 193–201, Sep. 2012.
- [10] E. E. J. Young, E. Mateeva, J. J. Moore, B. Mishra, and M. Loch, "Low pressure plasma spray coatings," *Int. Conf. Metall. Coatings Thin Film.*, vol. 377–378, no. 0, pp. 788–792, Jan. 2000.
- [11] M. Niittymäki, T. Suhonen, J. Metsäjoki, and K. Lahti, "Electric Field Dependency of Dielectric Behavior of Thermally Sprayed Ceramic Coatings," in *2015 IEEE 11th International Conference on the Properties and Applications of Dielectric Materials (ICPADM)*, 2015, pp. 500–503.
- [12] H. S. Khare and D. L. Burris, "A quantitative method for measuring nanocomposite dispersion," *Polymer (Guildf.)*, vol. 51, no. 3, pp. 719–729, Feb. 2010.
- [13] J. Ye, H. S. Khare, and D. L. Burris, "Quantitative characterization of solid lubricant transfer film quality," *Wear*, vol. 316, no. 1–2, pp. 133–143, Aug. 2014.
- [14] M. Niittymäki, K. Lahti, T. Suhonen, and J. Metsäjoki, "Dielectric Breakdown Strength of Thermally Sprayed Ceramic Coatings: Effects of Different Test Arrangements," *J. Therm. Spray Technol.*, vol. 24, no. 3, pp. 542–551, Jan. 2015.
- [15] M. Niittymäki, T. Suhonen, J. Metsäjoki, and K. Lahti, "Influence of Humidity and Temperature on the Dielectric Properties of Thermally Sprayed Ceramic MgAl2O4 Coatings," in *2014 Annual Report Conference on Electrical Insulation and Dielectric Phenomena*, 2014, pp. 94–97.